IMPACT OF NEUTRAL PARTICLES ON BEAM-ION LOSSES IN EAST TOKAMAK

Z. X. ZHANG, J. HUANG, J. F. CHANG, B. CAO, M. N. JIA, W. ZHANG, W. H. YE
Institute of Plasma Physics, Chinese Academy of Sciences
Hefei, China
Email: zixin.zhang@ipp.ac.cn

J. GALDON-QUIROGA
University of Seville,
Seville, Spain

A. SNICKER
VTT Technical Research Centre of Finland,
Espoo, Finland

Z. H. GAO, Z. X. WEN, S. Y. DAI
Dalian University of Technology
Dalian, China

Abstract

Experiments and simulations were conducted on the EAST tokamak to investigate the impact of neutral particle on beam-ion losses. In the experiments, supersonic molecular beam injection (SMBI) was applied during neutral beam heating to locally enhance the background neutral density. It was observed that SMBI from the J port significantly amplified the fast-ion loss detector (FILD) signal, whereas SMBI from the A port had little effect, highlighting the strong localization of beam-ion loss enhancement. To explain these observations, three-dimensional edge plasma and neutral distributions were reconstructed using EMC3-EIRENE with experimental profiles and subsequently used as input for the ASCOT5 simulations. A two-stage simulation scheme, including coulomb collisions, charge exchange and re-ionization, demonstrated that the high local neutral density generated by SMBI facilitates charge exchange of trapped beam ions in the scrape-off layer (SOL), producing fast neutrals that are not magnetically confined and directly strike the first wall. Furthermore, the re-ionization of fast neutrals was found to considerably modify the velocity-space distribution of lost ions, in agreement with FILD measurements. These results reveal that the relative geometric configuration of SMBI and NBI plays a decisive role in beam-ion losses, providing important guidance for optimizing fueling and heating system layouts to mitigate first-wall damage in future fusion devices.

1. INTRODUCTION

Achieving steady-state, high-performance operation and sustained fusion reactions in future fusion experimental reactors (ITER and CFETR) requires more than the ohmic heating generated by the plasma itself. Auxiliary heating is indispensable for reaching the temperatures necessary for fusion reactions. Currently, non-inductive heating methods mainly include radio-frequency (RF) heating and neutral beam injection (NBI) [1]. Among these, NBI has been widely employed as a primary plasma heating scheme in most fusion devices because it can provide controllable torque and drive off-axis current. Furthermore, density control and fuel retention are two critical challenges for future devices such as ITER, which aims to realize long-pulse, high-performance plasma discharges [2]. During plasma discharges, density can be sustained either through active fueling or, under saturated wall conditions, by particle recycling. When the recycling coefficient falls below unity, active fueling techniques such as gas puffing (GP), supersonic molecular beam injection (SMBI), and pellet injection can be employed to control plasma density.

However, interactions between beam ions and background neutrals enhance ion losses, which not only reduce the efficiency of NBI heating and plasma confinement, but in severe cases also cause first-wall damage that jeopardizes device operation [3–5]. A detailed understanding of interactions between beam ions and background neutrals is key to the effective mitigation of beam-ion losses. In this work, the effect of localized neutral density enhancement by means of SMBI on beam-ion losses is examined through a combination of experiments and numerical simulations in EAST tokamak. Three-dimensional background profiles are reconstructed using the EMC3-EIRENE code, and two-step orbit-following simulations with ASCOT5 are performed to elucidate the mechanism underlying the enhanced beam-ion losses observed by the fast-ion loss detector (FILD).

The remainder of this paper is organized as follows. Section 2 presents the experimental setup and results, including the configurations of NBI, SMBI, and FILD diagnostics on EAST, detailed discharge parameters, and

experimental observations of beam ion loss variations induced by SMBI at different injection locations. Section 3 describes the numerical simulations carried out to explain the experimental results, including the reconstruction of three-dimensional edge plasma and neutral density distributions with EMC3-EIRENE, their implementation as input for ASCOT5, and the analysis of wall load and velocity-space distributions of lost beam ions. Section 4 summarizes the main conclusions and discusses their implications for optimizing fueling and heating system layouts and mitigating beam ion–induced damage to plasma-facing components (PFCs) in future fusion devices.

2. EXPERIMENTAL DESCRIPTIONS

EAST is equipped with four NBIs that use deuterium as the working gas for auxiliary heating [6]. As shown in Fig. 1(a), the NBI system consists of two beamlines: NBI1 at the A port and NBI2 at the F port. Within these beamlines, NBI1R and NBI2L are configured for perpendicular injection in the co-Ip and ctr-Ip directions, respectively, whereas NBI1L and NBI2R are designed for tangential injection along the co-Ip and ctr-Ip directions. EAST is also equipped with two SMBI systems, namely SMBI3 at the A port and SMBI2 at the J port. Each system consists of a high-pressure gas source (1–2 MPa), electromagnetic valves, a Laval nozzle, and magnetic shielding. The Laval nozzle is mounted in front of the valves at approximately 2 m from the plasma. When subsonic gas passes through the Laval nozzle into the vacuum region, it forms a supersonic beam, allowing deeper penetration and more flexible density control compared with conventional gas puffing [2]. A scintillator-based FILD is installed at the J port to measure lost fast ions [7]. In the poloidal cross-section, the FILD is located near the midplane at z ≈ 0.224 m, and the detailed diagnostic parameters are provided in ref. [8].

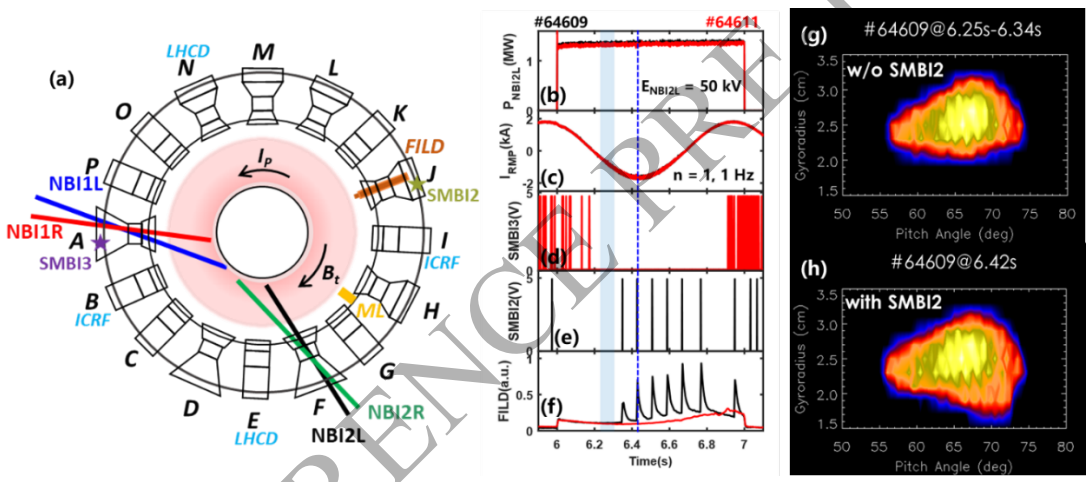

FIG. 1. (a) Layout of the auxiliary heating system, FILD and SMBI on EAST. Time evolution for discharges #64609 and #64611 of (b) NBI power, (c) RMP current, (d) SMBI3, (e) SMBI2 and (f) FILD signal. Beam-ion loss velocity-space distribution of #64609 (c) at 6.25s-6.34s (without SMBI) and (d) 6.42s (with SMBI).

To further investigate the impact of background neutrals on beam-ion losses, SMBI was employed to locally increase the neutral particle density in NBI experiments. The time evolution of discharges #64609 and #64611 is shown in Fig. 1(b)–(f). Both discharges have similar line-averaged densities ($n_e \sim 3.3 \times 10^{19}$ m^{-3}), NBI power ($P_{NBI2L} = 1.3$ MW, $E_{NBI2L} = 50$ kV), rotating RMP configuration (n = 1, 1 Hz), and plasma current ($I_p \sim 0.45$ MA), with the only difference being the SMBI location. As shown in Fig. 1(d)–(f), SMBI2 leads to a several-fold increase in the beam-ion loss signals measured by the FILD, whereas SMBI3 does not produce a noticeable change. These results indicate that SMBI induces localized enhancement of beam-ion losses, with further analysis presented in the following section. It is noteworthy that the magnitude of the loss enhancement depends on the phase difference between the upper and lower RMP coils, suggesting a synergistic effect between SMBI and RMPs. Furthermore, as shown in Fig. 1(g)–(h), SMBI2 also causes a broadening of the velocity-space distribution of lost beam ions, particularly in the region around pitch ~70° and gyro-radius ~2 cm.

3. SIMULATIONS

In this section, numerical simulations are employed to explain the experimental observations described above. Firstly, the three-dimensional (3D) background distributions induced by SMBI are obtained by combining experimental profile data with the 3D edge fluid transport code EMC3-EIRENE [9]. The resulting distributions of charged and neutral particles are then used as input background parameters for the test-particle orbit-following

code ASCOT5 [10]. Subsequently, a two-stage simulation scheme is implemented in ASCOT5 to achieve high-fidelity modeling of FILD signals with enhanced spatial and velocity-space resolution.

3.1. Three-dimensional distributions of background plasma and neutral particles

In tokamak devices, it is generally impractical to directly measure 3D background plasma parameters due to diagnostic limitations. Therefore, in this work, one-dimensional (1D) plasma profiles obtained from experiments are combined with EMC3-EIRENE simulations to reconstruct the 3D edge plasma parameters. In addition, the 3D distributions of background neutral particle density and temperature in the edge are obtained self-consistently based on the simulated plasma parameters. Fig. 2(a) shows the 1D plasma profiles of discharge #64609 at 6.20 s and 6.42 s, including electron density (from POINT and REF diagnostics), electron temperature (from TS and ECE), and ion temperature (from CXRS). The measured profiles are fitted and used in ONETWO to calculate the plasma stored energy, which agrees with experimental measurements within ~5%, ensuring the reliability of the plasma parameters. As seen in Fig. 2(a), SMBI2 causes a density increase in the edge region ($\rho > 0.9$), while the electron and ion temperature profiles remain unchanged. Based on experimental measurements, the total input power is approximately 1.98 MW, assumed to be equally distributed between electrons and ions. Impurity radiation power is subtracted from the total heating power, as the simulation focuses only on deuterium plasmas without impurities. According to the measured density at $\rho \sim 0.98$, the upstream densities are set to 1.1×10^{19} m^{-3} and 1.46×10^{19} m^{-3} for the without-SMBI and with-SMBI cases, respectively. By comparing with experimental profiles, the constant anomalous cross-field particle transport coefficient $D_\perp$ is determined as 0.15 m^2/s and 0.2 m^2/s for the without- and with-SMBI cases, respectively, while the cross-field energy transport coefficient $\chi_\perp$ is set to 3 m^2/s, as the background plasma temperatures remain nearly unchanged in both cases. Fig. 2(b) shows the poloidal distribution of electron density in the $\rho > 0.98$ region calculated by EMC3-EIRENE for the without-SMBI case. The reconstructed 3D background particle parameters, combining experimental data for $\rho < 0.98$ and simulation results for $\rho > 0.98$, are subsequently used as input for ASCOT5 simulations. Specifically, the 3D poloidal electron density distribution at the J port used in ASCOT5 for the without-SMBI case is shown in Fig. 3(a).

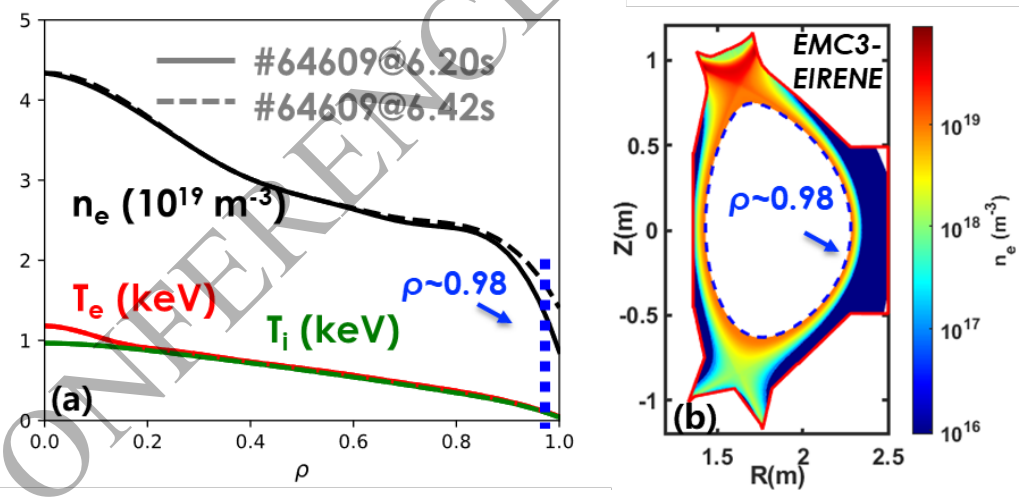

FIG. 2. (a) One-dimensional plasma profiles of EAST discharge #64609 at t = 6.20 s and 6.42 s. (b) Poloidal distribution of the edge electron density at the J port obtained from EMC3-EIRENE under the without-SMBI condition.

Fig. 3 shows the poloidal distributions of background particle densities at the J port. It can be seen that SMBI2 increases the electron density from ~10^{16} m^{-3} to ~10^{18} m^{-3} and the neutral particle density from ~10^{16} m^{-3} to ~10^{19} m^{-3}. In the simulations, the neutral particle density in the core region ($\rho < 0.98$) is set to a uniform value of 1×10^6 m^{-3}, as the core temperature is much higher than that at the edge. The toroidal distribution of background particle densities on a specific poloidal flux surface (indicated by the blue dashed line in Fig. 3(b)) is shown in Fig. 4. Since the relevant parameters of discharges #64609 and #64611 are nearly identical, the background particle density distribution for SMBI3 can be obtained simply by rotating the SMBI2 result by 175.5° along the toroidal direction. Fig. 4(a)–(c) indicate that SMBI only enhances the neutral particle density near the injection port. In contrast, the electron density distribution is enhanced along the entire toroidal direction due to parallel transport of charged particles along the magnetic field lines, as shown in Fig. 4(d)–(f).

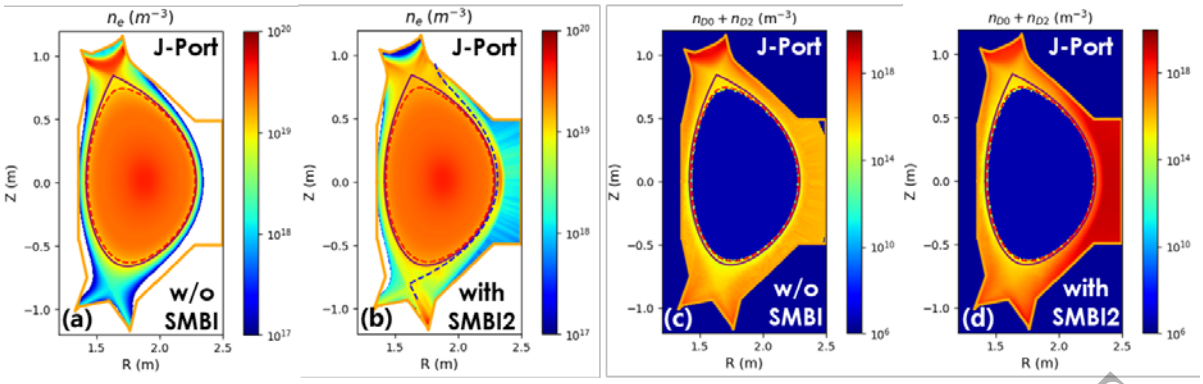

FIG. 3. Poloidal distributions of background particle densities at the J port obtained by combining experimental measurements and simulations. Poloidal distributions of background electron density under (a) without SMBI and (b) with SMBI2. Poloidal distributions of background neutral density (c) without SMBI and (d) with SMBI2.

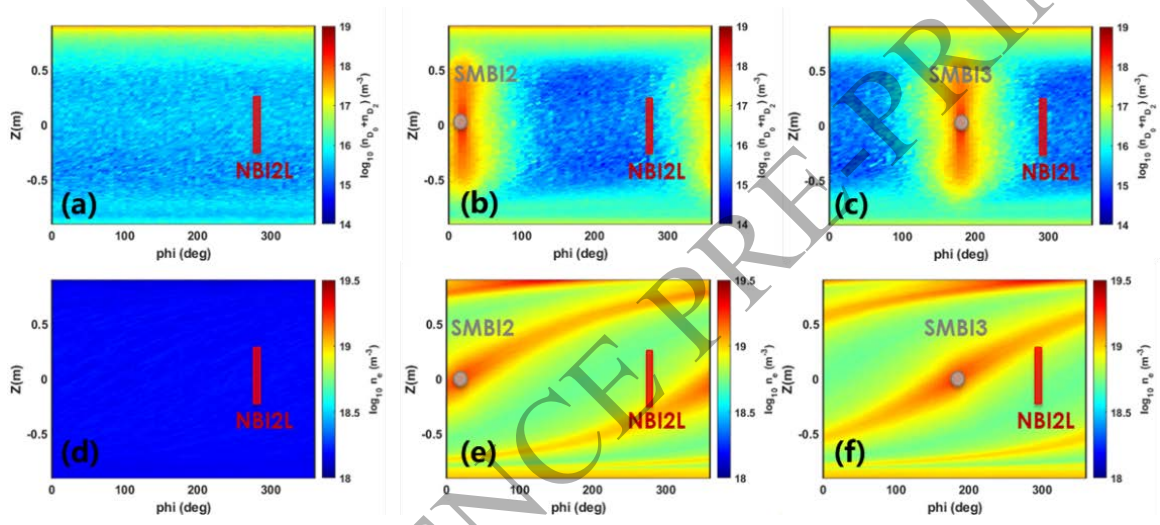

FIG. 4. Toroidal distributions of background particle densities on a specific poloidal flux surface (blue dashed line in Fig. 3(b)). Toroidal distributions of background neutral density under (a) without SMBI, (b) with SMBI2, and (c) with SMBI3. Toroidal distributions of background electron density under (d) without SMBI, (e) with SMBI2, and (f) with SMBI3.

3.2. Impact of SMBI on the spatial distribution of lost beam ions

Simulations were performed using the ASCOT5 orbit-following code, employing a two-stage scheme to enhance the fidelity of FILD signal modeling and improve resolution in velocity space. In the first stage, 10^7 markers representing initially deposited beam ions were generated using BBNBI. These markers were then tracked until they either reached the first wall, exceeded the maximum simulation time ($t_{lim} = 5\times10^{-4}$ s, much longer than the characteristic times τ_{CX} and τ_{re-ion} for charge-exchange and re-ionization reactions, respectively), or became neutralized by background neutrals. Full-orbit tracking was applied, with simulations including both Coulomb collisions and charge-exchange reactions [11]. Fig. 5 shows the poloidal and toroidal distributions of beam ions after one poloidal gyration period ($t=5\times10^{-4}$ s). Most beam ions remain confined within the plasma core. Passing beam ions are well-constrained in the core, whereas a significant population of trapped beam ions is located near the "banana tips," where parallel velocities decrease and perpendicular velocities increase. An example of a typical trapped ion orbit over one poloidal cycle is also shown, with the starting point located inside the LCFS near the beamline. The green line represents the inner leg of the orbit within the LCFS, while the red line corresponds to the outer leg outside the LCFS. When the starting point of a beam ion is closer to or beyond the LCFS, the ion is highly likely to be lost to the first wall during the first poloidal cycle, particularly in the "banana tip" region. Fig. 6(b)–(d) shows the wall-load distribution of lost beam ions in the first-stage simulations, both with and without SMBI. The results indicate that SMBI leads to increased wall loading near the beamline (around $\phi\sim290\circ$, $\theta\sim180\circ$). This is associated with the local enhancement of electron density near the beamline (F-port) induced by SMBI (Figs. 4(e) and 4(f)), which increases the fraction of initially deposited ions in the SOL (Fig. 6(a)). Beam ions deposited in the SOL can even be lost directly to the first wall along the inner leg of their orbits.

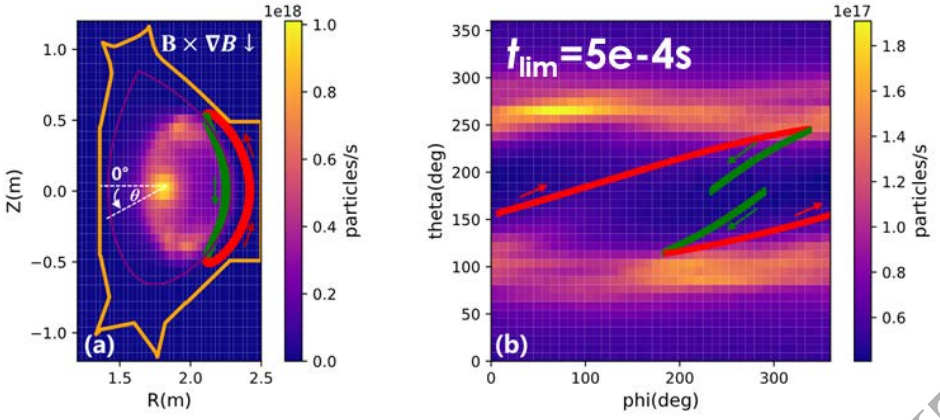

FIG. 5. Poloidal (a) and toroidal (b) distributions of beam ions after a gyro-orbit period with $t_{lim}=5\times10^{-4}$ s, obtained from ASCOT simulations. The green line indicates the inboard leg of a typical beam-ion orbit over one poloidal period, while the red line indicates the outboard leg.

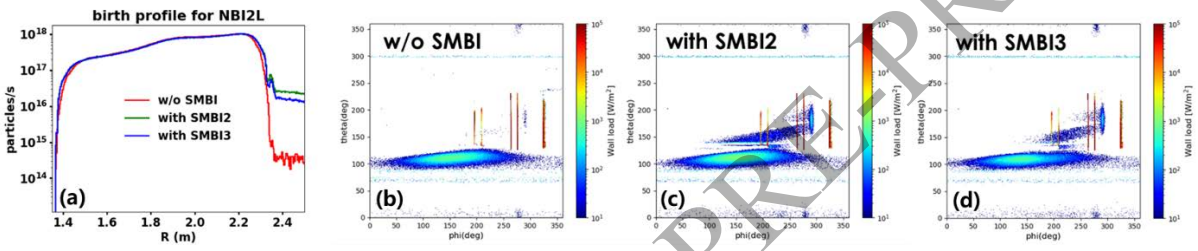

FIG. 6. (a) Initial deposition profile of NBI2L under without and with SMBI. Wall load distributions of lost beam ions from the first-step simulation (b) without SMBI, (c) with SMBI2, and (d) with SMBI3.

Fig. 7 illustrates the poloidal and toroidal distributions of fast neutral particle generation. In the present study, charge-exchange reactions of both atoms and molecules were included. Equation 3.1 describes the probability of a single beam ion being neutralized within a given simulation time step.

$$P(\delta t) = 1 - \prod_j \exp\left(-n_j \langle \sigma_j v \rangle \delta t\right) \qquad (3.1)$$

Here, n_j denotes the density of the corresponding neutral species, $\langle \sigma_j v \rangle$ represents the reaction rate coefficient for that species, and δt is the simulation time step. Fast neutrals are primarily generated in the SOL due to the higher background neutral density compared with the plasma core, as shown in Figs 7(a), (c), and (e). In the absence of SMBI, fast neutrals are mainly distributed toroidally near the "banana tip" region, where a large number of beam ions reside, even though the background neutral density in the SOL is relatively uniform. The introduction of SMBI leads to a several-orders-of-magnitude increase in the fast neutral generation rate compared to the baseline (without SMBI) case. Furthermore, the maximum fast neutral production is localized near the SMBI injection port. As shown in Fig. 7(d), SMBI2 induces fast neutral generation predominantly in the region with ϕ∼22.5∘ and θ∼180∘. This occurs because the outer leg of the trapped beam ion orbits intersects the SMBI2 location (Fig. 5(b)), leading to partial neutralization of beam ions near SMBI2. Similarly, Fig. 7(f) shows that SMBI3 results in fast neutral generation mainly in the region with ϕ∼180∘and θ∼110∘, as SMBI3 is positioned closer to the first "banana tip" region of the beam ions, where most trapped beam ions are neutralized. Comparing Figs. 7(b), (d), and (f), it is evident that SMBI3 produces the highest fast neutral generation rate due to the overlap between regions of high background neutral density and high beam ion population.

In the second stage of the simulation, the markers neutralized in the first stage were resampled. The number of markers representing fast neutrals was increased to 10^7 while their individual weights were correspondingly reduced. These markers were then tracked until they either reached the first wall or the simulation time limit ($t_{lim}=5\times10^{-4}$ s) was reached. Full-orbit tracking was employed, including Coulomb collisions, charge-exchange reactions, and re-ionization processes. The re-ionization processes accounted for interactions with background ions by BMS (from ADAS ADF21 format [12]) and with background neutrals by electron stripping (ES, including atomic and molecular contributions [13]). Figs 8(a)–(c) show the wall load distribution due to fast neutrals in the second-stage simulation. The results indicate that fast neutrals, being unconfined by the magnetic field, directly deposit on plasma-facing components (PFCs), and the peak wall load locations coincide closely with the peak fast

neutral production, i.e., near the SMBI injection port. Compared to the without-SMBI case, localized wall loads increase by approximately two orders of magnitude, which may pose a risk to diagnostics near the injection port. Figs 8(d)–(f) illustrate the wall load distribution caused by re-ionized beam ions. In the presence of SMBI, re-ionized beam ions enhance wall loads on the limiter; however, their contribution is significantly lower than that of fast neutrals. This is because a substantial fraction of re-ionized ions re-enter the LCFS and become well-confined beam ions again.

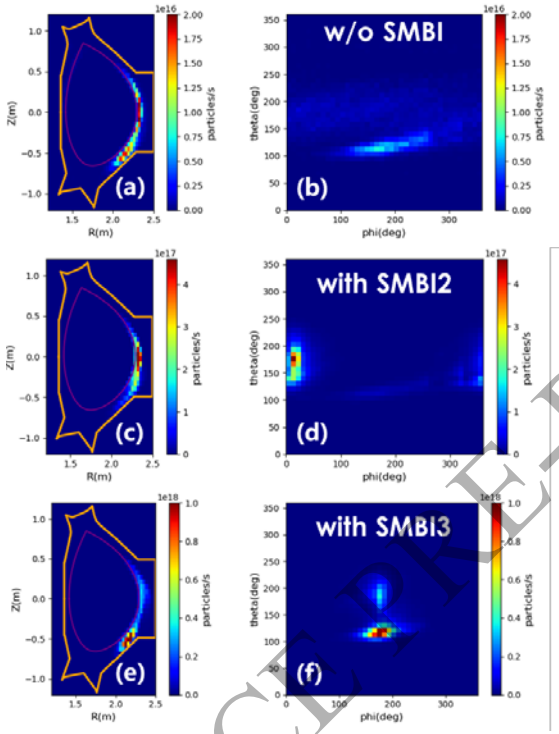

FIG. 7. Poloidal distributions of fast neutral generation rate (a) without SMBI, (c) with SMBI2, and (e) with SMBI3. Toroidal distributions of fast neutral generation rate (b) without SMBI, (d) with SMBI2, and (f) with SMBI3.

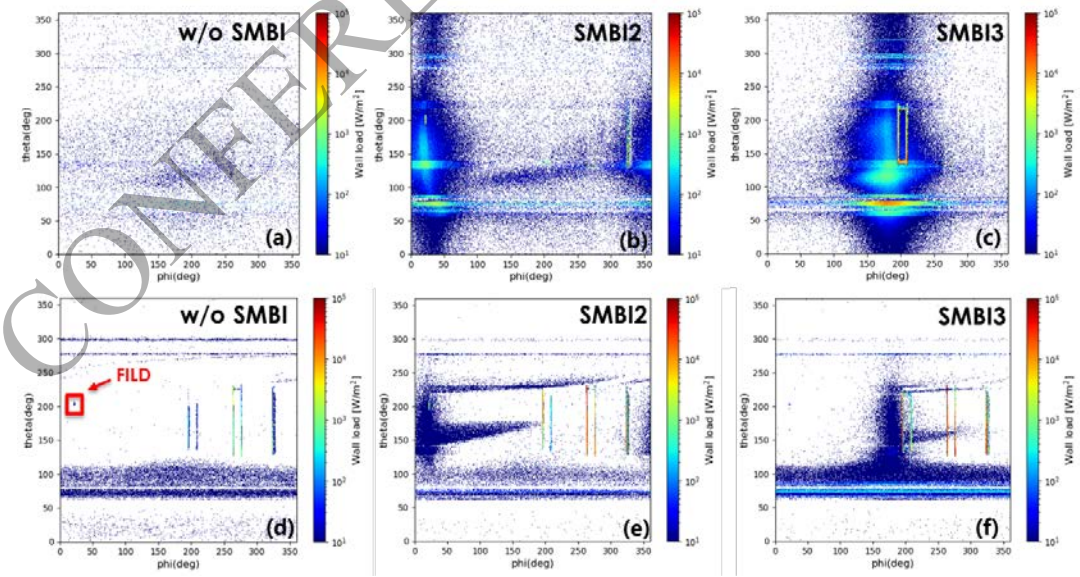

FIG. 8. Wall load distributions from the second-step simulation. Contributions from fast neutrals (a) without SMBI, (b) with SMBI2, and (c) with SMBI3 conditions. Contributions from re-ionized beam ions (d) without SMBI, (e) with SMBI2, and (f) with SMBI3.

3.3. Impact of locally enhanced neutral density on FILD signals

The previous sections have established the wall-load distributions caused by beam ions in the two-stage simulations. Subsequently, markers reaching the FILD (indicated by the red box in Fig. 8(d), $\varphi \sim 22.5°$, $\theta \sim 210°$) were collected and weighted to obtain the actual beam-ion loss rates. Fig. 9 presents the velocity-space distributions of beam ions lost to the FILD under different conditions. As shown in Figs. 9(a) and (d), The application of SMBI2 results in a pronounced broadening of the velocity-space distribution of FILD-detected beam-ion losses around pitch ~70° and elevates the corresponding loss rate by about fivefold, consistent with experimental measurements (Fig. 1). In contrast, SMBI3 does not cause a noticeable increase in the FILD-detected loss rate or velocity-space broadening, as shown in Fig. 9(c), because a substantial fraction of beam ions are lost near the SMBI3 location, reducing the losses near the FILD. It is noteworthy that neglecting the ES process during re-ionization leads to a reduction of the beam-ion loss rate by approximately 50% compared with the case including ES, as shown in Figs. 9(b) and (d). This highlights the non-negligible role of background neutrals in the re-ionization of fast neutrals.

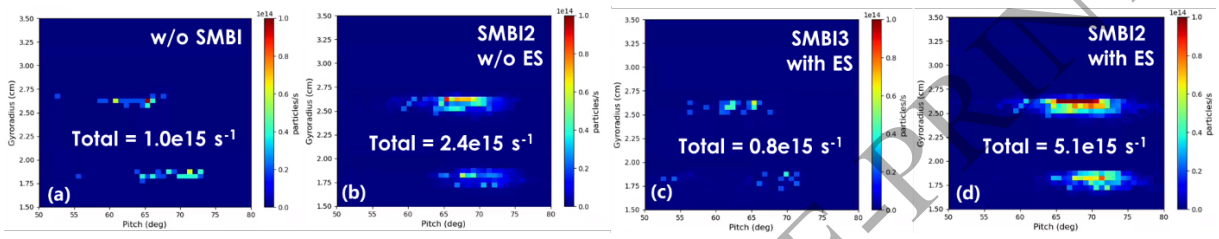

FIG. 9. Velocity-space distributions of beam ions lost to the FILD, obtained by collecting and weighting the two-step simulation results. (a) Without SMBI. (b) With SMBI2, neglecting the ES re-ionization process. (c) With SMBI3, including the ES re-ionization process. (d) With SMBI2, including the ES re-ionization process.

4. SUMMARY

This study combines experiments and simulations to investigate the impact of supersonic molecular beam injection (SMBI) on neutral beam ion losses in the EAST tokamak. Experimental results reveal a pronounced localized enhancement of beam-ion losses: SMBI injected at the J port significantly increases the loss signal detected by the FILD at that location, whereas SMBI at the A port produces no noticeable effect. To explain this behavior, three-dimensional background profiles, including electron and neutral densities, were reconstructed using the EMC3-EIRENE edge fluid transport code combined with experimentally measured one-dimensional profiles. The resulting self-consistent 3D background was used as input for test-particle orbit-following simulations with ASCOT5. The two-stage simulations elucidate the underlying physics: SMBI locally elevates neutral density at the plasma edge, causing beam ions in the SOL—particularly trapped beam ions—to undergo charge-exchange reactions, forming fast neutrals that are no longer confined by the magnetic field and are promptly lost to the first wall. The magnitude of this effect strongly depends on the spatial distribution of beam ions and the SMBI location. Furthermore, reionization due to background neutrals contributes non-negligibly to beam-ion losses and substantially broadens the velocity-space distribution of the lost ions. This study highlights that the relative geometry of key components, such as SMBI and NBI, critically influences beam-ion losses, providing important guidance for minimizing the impact of background neutrals and mitigating first-wall damage in future fusion devices.

ACKNOWLEDGEMENTS

Numerical computations were performed on the ShenMa High Performance Computing Cluster in the Institute of Plasma Physics, Chinese Academy of Sciences. This work is supported by the project National Key Research and Development Program of China No. 2019YFE03020004, the European Union under the Marie Sklodowska-Curie Grant Agreement No. 101069021, the Academy of Finland project No. 324759 and 362342.

REFERENCES

[1] HEIDBRINK W, SADLER G J., The behaviour of fast ions in tokamak experiments, Nuclear Fusion 34 (1994): 535

[2] ZHENG X, LI J, HU J, et al, Comparison between gas puffing and supersonic molecular beam injection in plasma density feedback experiments in EAST, Plasma Physics and Controlled Fusion, 55 (2013) 115010.
[3] DUONG H H, et al., Loss of energetic beam ions during TAE instabilities, Nuclear Fusion 33 (1993) 749
[4] KRAMER G.J., et al. Full-orbit simulations of fast-ion charge-exchange losses induced by neutral particles outside the last-closed flux surface Nucl. Fusion 60 (2020) 086016
[5] JAULMES F., et al., Modelling of charge-exchange induced NBI losses in the COMPASS upgrade tokamak, Nucl. Fusion 61 (2021) 046012
[6] FU J. et al., Characterization of beam ion loss in high poloidal beta regime on EAST, Plasma Phys. Control. Fusion 64 (2022) 095006
[7] CHANG J.F., et al., Scintillator-based fast ion loss measurements in the EAST, Rev. Sci. Instrum. 87 (2016) 11E728
[8] Z.X. ZHANG, et al., Experimental characteristics of lost fast negative ions on EAST tokamak, Nucl. Fusion 65 (2025) 046001
[9] J HUANG et al., Implementation and first application of EMC3-EIRENE to EAST double-null divertor, Plasma Phys. Control. Fusion 56 (2014) 075023
[10] HIRVIJOKI E. et al., ASCOT: solving the kinetic equation of minority particle species in tokamak plasmas, Comput. Phys. Commun. 185 (2014) 1310–21
[11] OLLUS P. et al., Simulating the impact of charge exchange on beam ions in MAST-U, Plasma Phys. Control. Fusion 64 (2022) 035014
[12] OLLUS P. et al., Validating the simulation of beam-ion charge exchange in MAST Upgrade, Plasma Phys. Control. Fusion 66 (2024) 025009
[13] BARNETT C.F. Collisions of H, H2, He, and Li Atoms and Ions with Atoms and Molecules, The Controlled Fusion Atomic Data Center, Oak Ridge National Laboratory (1990)